Journal of Applied Polymer Science

A Logistic Kinetic Model for Isothermal and Nonisothermal Cure Reactions of Thermosetting Polymers

Jorge López-Beceiro,[1] Sean A. Fontenot,[2] Carlos Gracia-Fernández,[3] Ramón Artiaga,[1] Richard Chartoff[2]

[1]University of A Coruña, Departamento de Ingeniería Industrial II EPS Avda. Mendizábal s/n, 15403 Ferrol, Spain
[2]CAMCOR Polymer Characterization Laboratory, University of Oregon, Eugene, Oregon 97403
[3]TA Instruments-Waters Cromatografía, Alcobendas 20108, Madrid, Spain
Correspondence to: R. Artiaga (E-mail: ramon.artiaga@udc.es)

ABSTRACT: A model describing the low-temperature crystallization kinetics observed for thermoplastic polymers from the melt by differential scanning calorimetry (DSC) was shown to accurately predict the cooling curves as a function of time and temperature. The model was successful for treating data for several cooling rates as well as for isothermal DSC data. In this article, we extended the model to cure reactions of thermosetting polymers. The parameters representing lower and upper exotherm reference temperatures in crystallization events have a different meaning for curing events. Thus, the model was modified to account for this change of context. The new model was tested for exothermic reactions of a Hysol® FP4527 epoxy adhesive system using data from DSC ramp heating experiments at several heating rates and also from isothermal experiments. Good fits were obtained for all the varied experimental conditions. The model made use of three fitting parameters with physical significance: a lower critical temperature (T_c) an activation energy (E_b), and a reaction order ($\tau + 1$). Additionally, to complete the kinetic fitting, the dependence of the time to reach the reaction peak maximum for isothermal cure was considered. That dependence was found to follow a more simple model which is formally equivalent to that observed in isothermal crystallization, and which makes use of two parameters related to the limits of the temperature range in which the polymerization may occur. © 2014 Wiley Periodicals, Inc. J. Appl. Polym. Sci. **2014**, *131*, 40670.

KEYWORDS: crosslinking; kinetics; thermosets

Received 7 December 2013; accepted 2 March 2014
DOI: 10.1002/app.40670

INTRODUCTION

Differential scanning calorimetry (DSC) is frequently used for the analysis of crystallization, melting, and curing processes. The most widely used procedures for determination of kinetic parameters for discrete curing reactions are model fitting and model-free procedures. Other approaches include time–temperature superposition kinetics[1] and master plots.[2,3] The conventional model-fitting approach assumes a fixed mechanism throughout the reaction, involving the fitting of conversion time data or rate of conversion-time data to some chemically based models to determine reaction orders, rate constants, and the activation energy from the Arrhenius equation.[4] An effective way to improve the goodness of fit is to flexibilize the model by introducing additional parameters. However, this tends to compromise the physical significance of the model.[4]

Crystallization and other liquid-to-solid transformations involving nucleation and growth are often described by the Kolmogorov–Johnson–Mehl–Avrami equation.[5–10] The model-free kinetic methods involve performing an isoconversional analysis on data taken at three or more heating rates, where the activation energy is allowed to vary with conversion.[11] Thus, model-free methods allow for a change of mechanism during the course of a reaction. Their suitability for obtaining activation energy values without modelistic assumptions is one of the reasons for their extensive use.[12–18] However, model-free methods have some disadvantages, and a reaction model is usually needed for a complete kinetic description of any liquid to solid state reaction.[14,19] It is also important to note that the model-free kinetic approach is usually applied in the context of the traditional kinetic description based on the kinetic triplet, A, E, and $f(\alpha)$ or $g(\alpha)$.[20] In that context, the temperature dependence is described by the Arrhenius equation

$$\frac{d\alpha}{dt} = A \quad \exp\left(\frac{-E}{R \quad T}\right) \quad f(\alpha)$$

where A and E (the pre-exponential factor and the activation energy, respectively) are Arrhenius parameters and R is the gas

constant. Thus, in practice, "free" refers only to the conversion (α) dependence and not to the temperature dependence, which is almost universally assumed to be described by the Arrhenius equation. Nevertheless, it would be risky to apply the Kolmogorov–Johnson–Mehl–Avrami model to cases where there is no evidence that the temperature dependence is accurately described by the Arrhenius equation. In such a situation, the A and E values estimated from the model would make no sense.

In the case of nonisothermal crystallization kinetics, the expression for the crystallized fractional volume contains a function of the initial temperature, and modifications of thermoanalytical models have been proposed to include that initial temperature effect.[21] The issues involved in modeling the liquid–solid state transformation kinetics, like heating or cooling rate, can exert a critical influence on the kinetic outcome. To account for this, a general methodology for nonisothermal transformations has been proposed.[22] On the other hand, the reliability of the data under analysis is an important aspect of any kinetic analysis, and obtaining a reliable baseline by means of a careful calibration is necessary.[23,24]

A previous study on the kinetic analysis of complex liquid to solid state transitions by a deconvolution procedure demonstrated that certain functions will properly fit the kinetic curves independently of the kinetics of the transformation, and the appropriate kinetic parameters can be obtained from a subsequent analysis.[25] A model proposed by the authors was conveniently adapted for the low temperature change of phase of a metal organic framework.[26] In implementing the model, a neat exotherm was obtained, which was not influenced by the heat capacity heat flow component. This exotherm was described by a generalized logistic derivative.

Further analysis of the parameter values obtained by the fitting yielded consistent kinetic information at three cooling rates. An interesting feature of that model is that it allows for determining a critical temperature, T_c, which is characteristic of the material and was related to the thermodynamic equilibrium transformation temperature.[26] However, in this form, the model could not be applied to isothermal data because it did not account for phase changes occurring with time at a constant temperature. The model was then modified so that the rate was expressed as a function of time and temperature. Thus, when applied to ramp data, the modified model not only matches the former one, but also fits isothermal data. The new model was then successfully applied to the crystallization from the melt of two polymers.[27] In this article, we adapted our model to a different process, the curing reactions of thermosets. In recent years, the study of cure kinetics of epoxy–anhydride systems was covered from different points of view, including phenomenological and mechanistically based models.[28–33] Mechanistically based models of different complexity were proposed for the curing kinetics and network buildup of epoxy–anhydride systems.[29] Nevertheless, a fully mechanism-based model that could explain the variety of experimental results found in the literature is still missing.[29] In general, model fitting approaches assumed an Arrhenius dependence of the reaction rate on the temperature and make use of some parameters to account for an autocatalytic effect. For example, it was suggested that the phenomenological two-parameter autocatalytic model is appropriate to describe the kinetics of the curing reaction of an epoxy–anhydride system in nonisothermal curing.[33] Other authors preferred the more flexible Kamal model for isothermal and nonisothermal experimental data. In this case, two activation energies, two pre-exponential factors, and two exponents were adjusted by multivariate nonlinear regression.[28] Other studies revealed that curing propagation mainly occurs by polyesterification between epoxide and anhydride and some autocatalysis may occur, but this is a minor contribution to the kinetics of cure. The ester formation follows first-order kinetics up to the point where the reaction becomes diffusion controlled (about 70%) with an Arrhenius dependency of the rate coefficient on temperature.[31] An interesting approach consisted of including both chemical- and diffusion controlled stages of reaction in a model derived from the Sestak–Berggren one where it was assumed that the autocatalytic phenomenon results from the difference of kinetics between the initiation and propagation stages or other reaction mechanisms.[30] Another model consisting of a reversible reaction transforming an inactive species into an active one and the usual propagation step was adjusted by multiparametric regression. Several sets of values provided reasonable fits of the DSC scan, and one of these sets explained most of the experimental findings reported in the literature.[32] It was also mentioned that isoconversional methods should not be applied to obtain fundamental kinetic parameters in systems where the reaction rate depends on the concentration of an active species that varies independently of the conversion of functional groups.[32] In spite of the physical interpretation of some of the mentioned methods, the quality of the fittings obtained up to the moment is still not good enough to be blindly trusted. In this case, on adapting the aforementioned model proposed by the authors for polymer crystallization, the reference temperatures need to be redefined because of the opposite effects of temperature on the rate of curing compared with the effects on the crystallization rate. We tested this revised model with the isothermal and nonisothermal curing of an epoxy resin system.

EXPERIMENTAL

The thermoset epoxy resin, Hysol® FP4527, was used for this study. This epoxy is based on the diglycidyl ether of bisphenol-A and contains a mixture of hexahydromethylphthalic anhydride and methyltetrahydrophthalic anhydride as hardeners. Filler content, determined by thermogravimetric analysis (TGA), was found to be 68%. DSC experiments were carried out in a TA Instruments Q2000 MDSC equipped with an RCS-90 cooling system. Hysol® samples were stored at or below −60°C, and all experiments were performed in a nitrogen atmosphere. Samples were weighed directly into T-zero Aluminum pans which were crimped. The pans were re-weighed after each experiment to verify that the sample masses remained constant over the course of the experiment. Sample sizes ranged from 3.98 to 10.82 mg. Although mass–rate compensation was recommended to prevent problems such as lack of sensitivity and peak broadening,[34] previous tests performed on this instrument demonstrated that the sensitivity is sufficient at all heating rates. The DSC instrument accounts for the thermal resistance and capacitance of the cell, pans, and thermocouple–pan interfaces. The peak broadening

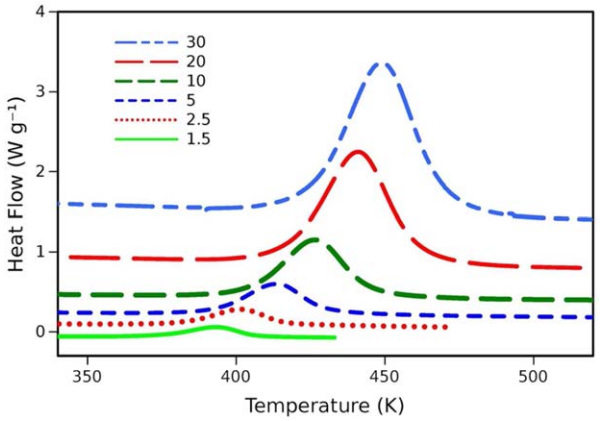

Figure 1. Heat flow curves versus temperature obtained at different heating rates. [Color figure can be viewed in the online issue, which is available at wileyonlinelibrary.com.]

was minimized by using small sample sizes. Ramp experiments were performed with heating rates of 1.5, 2.5, 5, 10, 20, and 30°C/min. Isothermal experiments were performed at temperatures of 95, 105, 110, 120, and 130°C. Isothermal temperatures were reached by rapidly heating at 80°C/min to the designated test temperature. TGA experiments were performed using a TA Instruments Q500 TGA in high resolution mode with air as the sample purge gas. For all TGA and DSC experiments, calibrations were performed as recommended by the instrument manufacturer.

RESULTS

Figure 1 is an overlay of the heat flow curves obtained from the ramp heating experiments. The positions of the cure exotherms on the temperature axis are dependent on the heating rate, which is normal for typical thermosets. Figure 2 shows the DSC heat flow and temperature curves obtained from an isothermal experiment at 130°C. The transition from the heating ramp to isotherm was not instantaneous, and a slight overheating was observed immediately following the ramp. However, the maximum deviation from the programmed isothermal temperature due to this overheating was only 0.05°C, which has little effect on the reaction rate.

Adapting the Crystallization Model to Thermoset Curing

The approach used in our previous work assumes that the overall crystallization process takes place if the material is held at a temperature at which the process can occur. In that case, the beginning of crystallization is an asymptotic process and establishing a discrete induction time would make no sense. Thus, instead of the induction time, the peak time or isothermal time to the maximum crystallization rate, t_{piso}, was chosen to evaluate the effect of temperature on the bulk crystallization rate. In this report, we use a similar approach for curing reactions. However, the reference temperatures need to be redefined, because the effects of temperature on the crystallization rate and on the curing rate are opposite (an increase in temperature produces a decrease in the crystallization rate and an increase in the curing rate).

Two important differences between the cure process and crystallization process are as follows:

- In nonisothermal crystallization, the change in C_p (excluding the heat flow involved in the first order transition) is continuous and proportional to the conversion, α. In a curing system, change in C_p depends also on whether or not the heating rate is high enough to prevent vitrification before completion of the cure.
- Similar degrees of crystallization are observed in isothermal experiments performed at different temperatures. But, the maximum degree of curing depends strongly on the temperature.
- If the heating rate is not high enough, it is possible that some deviations from linearity of C_p occur as a consequence of the vitrification and devitrification processes, which would result from the simultaneous changes in the degree of crosslinking and temperature with time.[35] The heating rates used in this work allowed us to obtain curing peaks free from shoulders. This is an indication that there were no intercalated vitrification and devitrification processes.

The New Model

Our model was initially developed for ramped cooling experiments in which a change of baseline was expected resulting from the change of temperature and the change of heat capacity due to the first-order transformation of the material.[26] Two straight lines, $y_1(T)$ and $y_2(T)$ reproduced the baseline slopes before and after the transition. The baseline change due to change in heat capacity was modeled by a generalized logistic function, $y_3(T)$. This function, when resized to the asymptotic values of 1 and 0, represents the untransformed fraction of the sample. The nonreversing heat flow component, which represents the heat flow due to a firs-order transition, was modeled by the first derivative of a generalized logistic function, $y_4(T)$. A further revision of the model accounts for the time effect and can be applied to both ramp and isothermal kinetics.[27] In its present form, the model is represented by a mixture of the functions of time, listed in Table I, being eq. (1) a generalized logistic function and eq. (2) the time derivative of eq. (1). The m_t parameter represents the time at the maximum rate of change, b_t is related to the rate of change, τ_t accounts for the asymmetry, c_t represents the peak area, and t is the time,

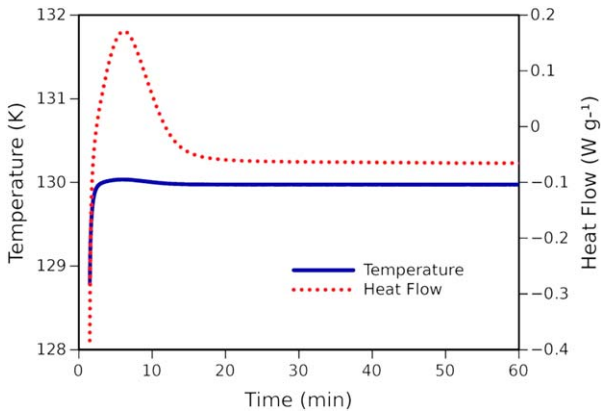

Figure 2. DSC curve and temperature profile for an isothermal heating experiment at 130°C. [Color figure can be viewed in the online issue, which is available at wileyonlinelibrary.com.]

Table I. Functions Used in the Model

$y_1(t)=k_{1t}+s_{1t}\cdot t$
$y_2(t)=k_{2t}+s_{2t}\cdot t$
$y_3(t)=\frac{1}{[1+\tau\cdot\exp(-b_t\cdot(m_t-t))]^{1/\tau_t}}$ (1)
$y_4(t)=\frac{c_t\cdot b_t\cdot\exp(-b_t\cdot(m_t-t))}{[1+\tau_t\cdot\exp(-b_t\cdot(m_t-t))]^{(1+\tau_t)/\tau_t}}$ (2)
$y_3(t,\alpha)=(1-\alpha)$ (3)
$y_4(t,\alpha)=c_t\cdot b_t\cdot\exp(-b_t\cdot(m_t-t))\cdot(1-\alpha)^{1+\tau_t}$ (4)

measured from the beginning of the experiment. The heat capacity component was described by this expression:

$$y_{rev}(t)=y_1(t)+[y_2(t)\quad y_3(t)]$$

and the model was expressed as:

$$y_{tot}(t)=y_1(t)+[y_2(t)\quad y_3(t)]+y_4(t)$$

where $y_{total}(t)$ represents the estimated heat flow.

As mentioned, the generalized logistic function, $y_3(t)$, represents the untransformed fraction of the sample $(1-\alpha)$. Thus, $y_4(t)$, the nonreversing heat flow component, can be represented as a function of the conversion, as expressed in eq. (4). Considered as a model to fit single DSC curves, the proposed model, as described by eq. (4), has one more parameter than the standard Arrhenius-reaction order 1. Nevertheless, two of the parameters of the proposed model (m_t, the time at the maximum of the DSC peak, and c_t, the area of the peak) practically do not contribute to the flexibility of the model because their values are practically independent from the other parameters and can be determined without performing any fitting. Thus, m_t and c_t do not compromise the physical significance of the other parameters, b_t and τ_t.

For isothermal transformations any possible change of the baseline would be negligible and thus a flat baseline is assumed. Consequently, in the isothermal case, the model consists of only the $y_4(t)$ function. Nevertheless, it has to be taken into account that eqs. (1) and (2) can be applied to both isothermal and nonisothermal processes, but the physical meaning of the parameters involved in isothermal and nonisothermal conditions is different, except for τ, as it will be commented later. Thus, from now on, the subscripts *iso* and *ramp* will be used to identify isothermal and heating ramp conditions, respectively. Accordingly, the b_t parameter is the one that contains the most significant kinetic information. The following relation for b_t was proposed for ramp experiments and seemed to work very well:

$$b_{tramp}=\frac{E_{bramp}}{R\quad t_{pramp}\quad T_c} \quad (1)$$

where T_c is the critical temperature for the process to occur (this is discussed below), t_{pramp} represents the time elapsed from T_c to the instant where the maximum rate of change occurs, E_{bramp} is an apparent energy barrier, and R is the gas constant. A formally equivalent relation is assumed for isothermal conditions:

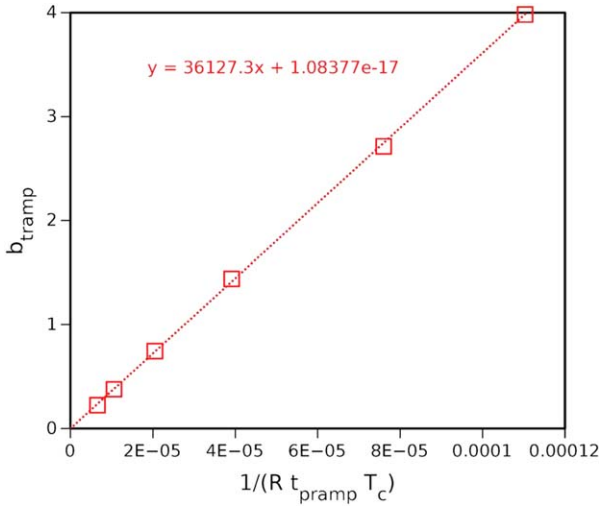

Figure 3. Plot of the b_{tramp} values obtained from the fitting of the single heat flow curves versus $1/(R\ t_{pramp}\ T_c)$. [Color figure can be viewed in the online issue, which is available at wileyonlinelibrary.com.]

$$b_{tiso}=\frac{E_{biso}}{R\quad t_{piso}\quad T_c} \quad (2)$$

Consequently, and assuming that, although the meaning of the parameters is different, the relations of the parameters are formally identical in isothermal and nonisothermal contexts, the model can be written as a non-Arrhenius reaction order 1:

$$y_4(t,\alpha)=c_t\quad\frac{E_b}{R\quad t_p\quad T_c}\quad\exp\left(\frac{-E_b}{R\quad T_c}\quad\frac{m_t-t}{t_p}\right)\quad(1-\alpha)^{1+\tau_t} \quad (3)$$

where E_b has dimensions of enthalpy. Equation (3) applies to isothermal and nonisothermal data, but the E_b parameter has a different meaning in the isothermal case, E_{biso}, than in ramp, E_{bramp}. The value of t_{pramp} is always higher than the isothermal peak time obtained at the same temperature at which the ramp peak was observed, and, consequently, E_{bramp} is higher than E_{biso}. It can be easily inferred that the higher the E_{bramp}/E_{biso} rate, the higher the accelerating effect of the temperature on the curing rate. According to eq. (3), in ramping, the exponential

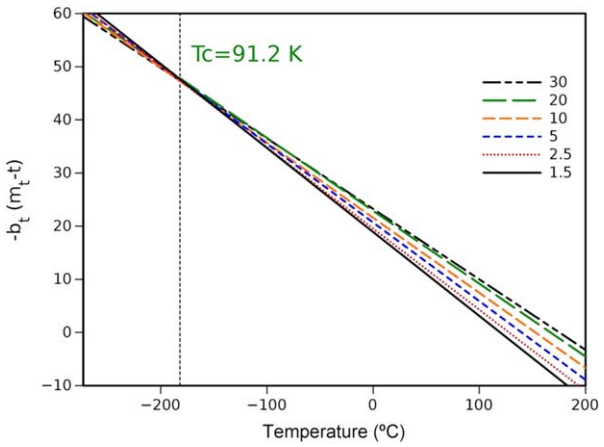

Figure 4. Exponential terms of $y_4(t)$ versus temperature obtained at the indicated heating rates. [Color figure can be viewed in the online issue, which is available at wileyonlinelibrary.com.]

Table II. Parameter and R^2 Values Obtained from Fitting the Ramp Heat Flow Curves to the Model

	Heating rate (K min^{-1})					
	1.5	2.5	5	10	20	30
c_t (W min g^{-1})	1.5513	1.5899	1.6324	1.7655	1.9637	1.8433
τ	0.3704	0.4623	0.5808	0.7313	0.9406	0.9541
b_t (min^{-1})	0.2370	0.3820	0.7401	1.4136	2.7462	3.9860
Enthalpy (J g^{-1})	291	298	306	331	368	346
m_t (min)	193.85	38.78	21.84	12.29	6.92	4.94
T_p (K)	392.83	401.18	413.11	426.27	440.36	448.58
R^2	0.9992	0.9998	0.9998	0.9998	0.9995	0.9949

The enthalpy values, calculated from c_t, refer to the polymer fraction. The T_p value is the instantaneous temperature at m_t.

term is formally (because E_{bramp} is not the true energy barrier) equivalent to that of Arrhenius only at the instance where $T = T_c$, where $(m_t - t) = t_p$. A true Arrhenius dependence would be observed only, according to the exponential term of eq. (3), at the beginning of a hypothetical isothermal case at $T = T_c$. It is also clear that, both in ramp or isothermal conditions, the exponential term becomes equal to 1 at the peak, because $t = m_t$. On the other hand, because $y_4(t,\alpha)$ is function of the unreacted mass, $(1 - \alpha)$, the model is a reaction order 1, and the reaction order is represented by $1 + \tau_t$. The T_c parameter represents an important difference with respect to classical Arrhenius-based models. The Arrhenius model assumes a Maxwell–Boltzmann distribution for the fraction of molecules with energy greater than a given energy barrier named "activation energy." Accordingly, any process would take place, although at low temperature the rate would be low, at any temperature above 0 K. Nevertheless, the model presented here assumes that there is a minimum temperature, T_c, for each process and that no process can proceed at temperatures below its T_c.

The Fitting Procedure

The fitting methodology was explained in our previous work.[26,36] It consists of fitting the baseline at both sides of the peak by means of two straight lines, $y_1(t)$ and $y_2(t)$, and then fitting the peak region by introducing the $y_3(t)$ and $y_4(t)$ functions, which are a generalized logistic function and its derivative, respectively. The fitting was optimized by minimizing the sum of squared residuals, which is a method widely used.[37–39] Fityk software was chosen to perform this task.[40] The $y_{rev}(t)$ function provides a good approach for describing the C_p change occurring during the ramp experiments, whereas a flat baseline is preferred for isothermal experiments. A few data at the beginning of the isothermal heat flow curves were not included in the fittings because the heat flow measurements are not very reliable until the temperature is stabilized.

Linear Ramp Heating Experiments

It was shown in our previous work that when a process follows the $y_4(t)$ model, the plots of the exponential term of $y_4(t)$, using the parameter values obtained at several heating rates, versus T, cross approximately at the same point, named the critical temperature, T_c.[27] Accordingly, plots of the exponential term of $y_4(t)$ versus temperature should cross at T_c. In this case, parameter values were obtained by the fitting $y_4(t)$ to the single heat flow curves obtained in ramping. Assuming the relation expressed by eq. (1) and considering that

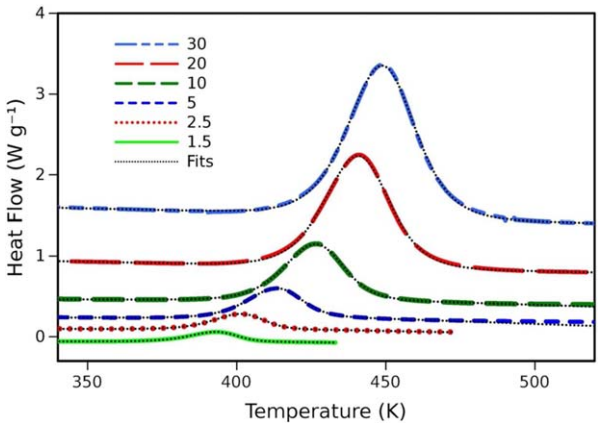

Figure 5. DSC curves obtained at several ramp heating rates and the corresponding model results. The curves were shifted on the heat flow axis and overlaid for easier observation. [Color figure can be viewed in the online issue, which is available at wileyonlinelibrary.com.]

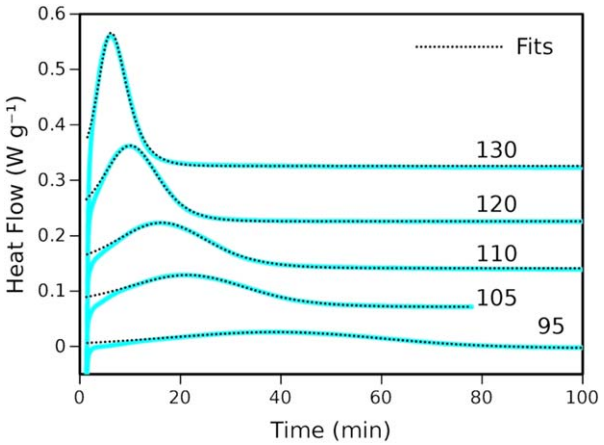

Figure 6. Plots of DSC curves and their corresponding model fits obtained for isothermal experiments. The isothermal temperatures are indicated. The data are shifted and overlaid on the heat flow axis for easier observation. [Color figure can be viewed in the online issue, which is available at wileyonlinelibrary.com.]

Table III. Parameter Values Obtained from Fitting the Isothermal Heat Flow Curves to the Proposed Model

	Isothermal temperature (K)				
	368.15	378.15	383.15	393.15	403.15
c_t (W min g^{-1})	1.7437	1.8378	2.0238	1.9326	1.8927
τ	0.6346	0.8537	1.0525	1.2689	1.3679
b_t (min^{-1})	0.0598	0.1194	0.1657	0.3091	0.5538
Enthalpy (J g^{-1})	327	345	379	362	355
R^2	0.9997	0.9994	0.9993	0.9993	0.9942

$$t_{\text{pramp}} = \frac{T_p - T_c}{\text{HR}} \quad (4)$$

where T_p is the peak temperature and HR the heating rate, optimal values of E_{bramp} and T_c were found. Figure 3 shows how the b_{tramp} values obtained from the fitting of the single ramp heat flow curves fall practically in a straight line when plotted versus $1/(R\ t_{\text{pramp}}\ T_c)$. Then, the b_{tramp} values were slightly adjusted to fall exactly on the straight line, and the single ramp heat flow curves were fitted again by locking these adjusted b_{tramp} values and allowing the remaining parameter values to vary. The resulting values of T_c and E_{bramp} were 91 K and 36,127 J/mol. Figure 4 shows how the plots of the exponential term of $y_4(t)$ versus temperature cross exactly at T_c. The parameter values and the determination index, R^2, resulting from the fitting of the heat flow curves are shown in Table II.. The quality of fit is very good because the determination index is very close to 1 and, according to Figure 5, the fits match the experimental DSC curves perfectly.

Fitting of Isothermal Data: Functional Dependence of the Peak Time

The $y_4(t)$ expression was fit to the isothermal DSC curves. The fitting covered in all cases a broad range of conversions from near the beginning of the isotherm to a point where the DSC curve diminished to a virtually flat baseline. Figure 6 shows that good fits were obtained at all isothermal temperatures.

Table III shows the corresponding values of the fitting parameter and the coefficient of determination, R^2, obtained from the isothermal curves. The enthalpy values obtained from isothermal experiments are similar to those obtained from ramp experiments. Once a reliable fit is obtained, the subsequent kinetic analysis yields the correct kinetic parameters.[25]

The following functions were chosen for the peak time, t_{piso}, and the b_{tiso} parameters for the original isothermal crystallization model:

$$t_{\text{piso}} = t_{\text{Tb}} \quad \exp \frac{(T - T_b)}{(T_c - T)} \quad (5)$$

$$1/b_{\text{tiso}} = 1/b_{T_b} \exp \frac{(T - T_b)}{(T_c - T)} \quad (6)$$

where T_c is the critical temperature and T_b, t_{Tb}, and b_{Tb} are fitting parameters. T_c represents a temperature at which the curing would take an infinite time and below which no curing would occur. Although T_b represents the temperature at which the time to reach the peak would be very small, t_{Tb}, it does not represent any behavioral frontier but is only a reference temperature for the exponential term becoming lower or higher than 1. It is important to note that the critical temperature, T_c, for crystallization is the higher reference temperature, whereas in curing, the critical temperature is the lower one. Similarly, the other reference temperature, T_b, is the lower reference temperature in crystallization but the higher reference temperature in curing. Figure 7 plots the t_{piso} and $1/b_{\text{tiso}}$ values, obtained from isothermal

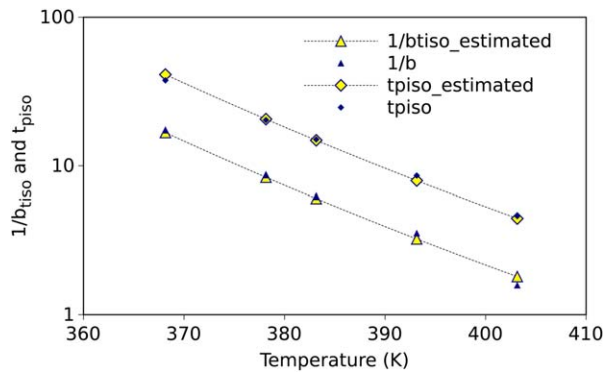

Figure 7. Plots of t_{piso} and of $1/b_{\text{tiso}}$ obtained from isothermal curing experiments versus the isothermal temperature. Optimal fitting of the data to eqs. (5) and (6) are also shown. [Color figure can be viewed in the online issue, which is available at wileyonlinelibrary.com.]

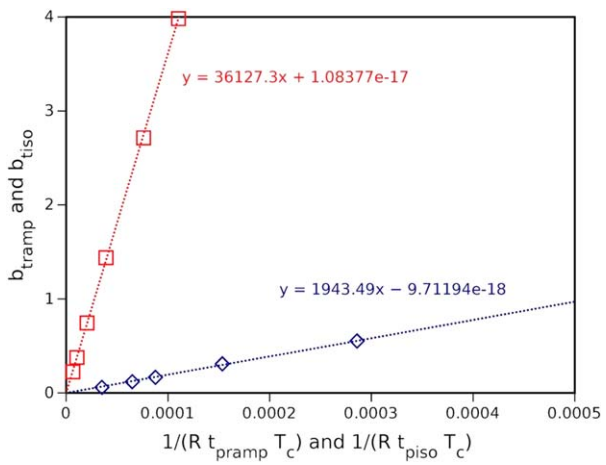

Figure 8. Plot of the b_{tramp} and b_{tiso} parameter values versus $1/(R\ T_c\ t_{\text{pramp}})$ and $1/(R\ T_c\ t_{\text{piso}})$, respectively. [Color figure can be viewed in the online issue, which is available at wileyonlinelibrary.com.]

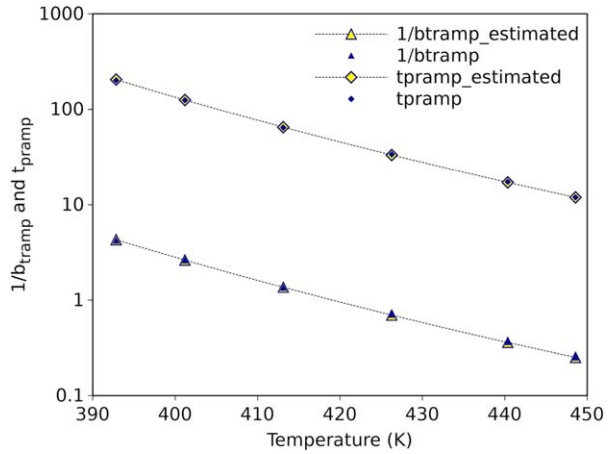

Figure 9. Plots of t_{pramp} and of $1/b_{tramp}$ obtained from nonisothermal curing experiments, versus the peak temperature. Optimal fitting of the data to eqs. (5) and (6) are also plotted. [Color figure can be viewed in the online issue, which is available at wileyonlinelibrary.com.]

cures, versus the temperature. The dependence represented by eqs. (5) and (6) is proposed for these parameters. Assuming the T_c values obtained from the ramp experiments, optimal fits of these parameters to the experimental results are presented in Figure 7. The optimal values of T_b, t_{Tb}, and $1/b_{Tb}$ were obtained by minimizing the weighted sum of squared residuals. The fact that we have obtained very good fits with a model that represents a single process is an indication that, in the case where more than one process is occurring, either they are all simultaneous or one of them is much more dominant than the others. It is observed that t_{piso} is proportional to $1/b_{tiso}$.

$$t_{piso} = 2.46\frac{1}{b_{tiso}}$$

We would like to emphasize that the parameters of eq. (2) are not the same (because their physical meanings are different) in isothermal and nonisothermal contexts. The reason why this is so is that the time measured in ramp cannot be taken as equivalent to the time elapsed under isothermal conditions. The only parameter in common (formally and physically) is τ: in both cases the unreacted fraction is raised to the same power $(1+\tau)$, which can be understood as a reaction order. Furthermore, τ represents the asymmetry of the process (mathematically, $\tau = 1$ corresponds to perfect symmetry). Thus, it is not surprising that the values of τ obtained in isothermal conditions vary with temperature and those obtained in ramp vary with the heating rate. On the other hand, T_c can be obtained as a cross point from the fittings obtained at several heating rates and also from isothermal experiments through eqs. (5) and (6). The fact of obtaining a T_c value that agrees with both isothermal and nonisothermal approaches supports the reliability of this parameter.

Energy Barrier and Heating Rate Considerations

Although the mathematical expressions used to represent the process for both isothermal and ramp conditions were formally equivalent, the parameters obtained for both conditions were not the same. Figure 8 shows the b_{tiso} values versus $1/(R\ T_c\ t_{piso})$ and b_{tramp} versus $1/(R\ T_c\ t_{pramp})$ obtained from isothermal

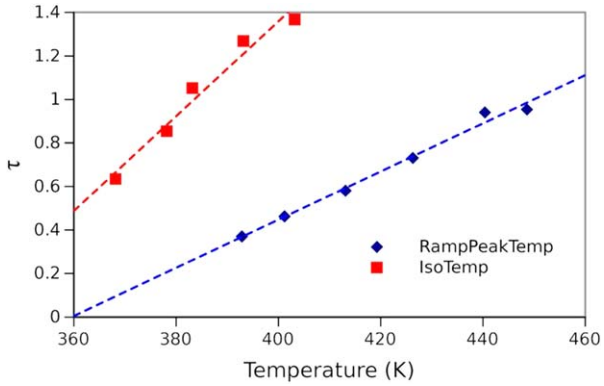

Figure 10. Plots of τ versus the peak temperature obtained in ramp and in isothermal tests from Hysol FP4527. [Color figure can be viewed in the online issue, which is available at wileyonlinelibrary.com.]

and nonisothermal data. The slope of the isothermal line, E_{biso} represents the energy barrier of the curing reaction. The value obtained was 1943 J mol^{-1}. The slope of the nonisothermal line, E_{bramp}, gave 36,127 J mol^{-1}. As mentioned before, E_{bramp} was always higher than E_{biso} because t_{pramp} was always higher than the isothermal peak time obtained at the same temperature at which the ramp peak was observed. The E_{bramp}/E_{biso} rate (in this case 18.6) was related to the accelerating effect of the temperature on the curing rate. These values cannot be compared with activation energy values obtained assuming a different dependence (for example using Arrhenius based models) on temperature but would be surely useful to make comparisons when this very model is applied to other curing systems.

In view of the results explained above it was possible to calculate T_c and E_{bramp} from only two ramp experiments, as commented on the description of Figure 3. Provided the T_c value obtained from ramp, E_{biso} can be then calculated from a single isothermal experiment. This experiment should be performed at a relatively high temperature (higher b_{tiso}) to minimize the effect of any possible experimental error on the slope, as it can be derived from Figure 8.

Parameter Trends and Predictions

An applicative outcome of the results presented here is the possibility of doing predictions of the curing rate in different

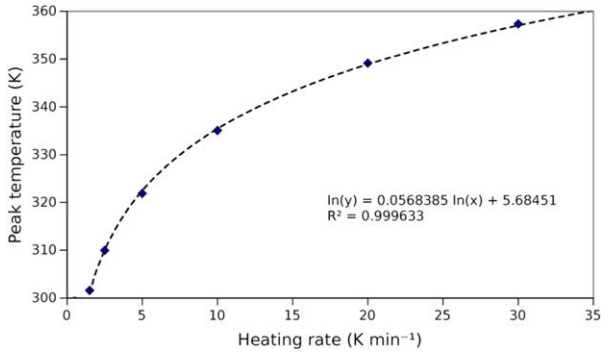

Figure 11. Plot of the peak temperature values obtained in the fitting of single curves versus the heating rate. [Color figure can be viewed in the online issue, which is available at wileyonlinelibrary.com.]

thermal conditions. To make predictions at different isothermal temperatures or different heating rates it is necessary to know the critical temperature, the true and apparent energy barriers, and how the peak time and the reaction order change with the isothermal temperature and the heating rate. In isothermal conditions, the peak time was observed to follow the trend described by eq. (5), which is represented in Figure 7. The trend of the peak time, and also of $1/b$, in ramp experiments followed the same trend but with a different preexponential factor, as can be observed in Figure 9. The model had the mathematical form of a reaction order expression, whereas the reaction order, $1 + \tau$, was found to depend on the heating rate. Linear trends of τ were observed in the experimental range with respect to the ramp peak and isothermal temperatures, as depicted in Figure 10, although it is still unclear how the reaction order changes outside of the experimental range and extrapolation might be risky. Although the relation between the peak temperature and the heating rate can be indirectly obtained from the trends of t_{pramp} versus the peak temperature obtained in ramp, presented in Figure 9, and that of peak time and peak temperature with the heating rate, represented by eq. (4), Figure 11 shows that this relation clearly follows a power law trend.

CONCLUSIONS

A kinetic model, which was originally used to describe both the low temperature transformation of a metal organic compound and polymer crystallization from the melt state, was adapted for and tested on isothermal and nonisothermal curing of thermosets. The model, based on generalized logistic functions, is a non-Arrhenius reaction order model. It allows for determination of the energy barrier of the process from isothermal experiments. A different energy barrier parameter was observed in ramp experiments, which accounted for a progressive acceleration as the temperature increased. It is still unclear how the reaction order changes outside of the experimental range. Thus, it is unsafe to extrapolate this parameter for temperatures outside of the experimental range. It is possible to calculate the energy barrier parameters and the critical temperature from only one isothermal experiment (preferably performed at a relatively high temperature) and two ramp experiments. The fact that we have obtained very good fits with a model that represents a single process is an indication that, in the case where more than one process is occurring, either they are all simultaneous or one of them is much more dominant than the others. The model had the mathematical form of a reaction order expression, whereas the reaction order was found to depend on the heating rate.

ACKNOWLEDGMENTS

The authors acknowledge the Spanish Ministerio de Ciencia e Innovación for the provision of funds MTM2011–22392. The authors also acknowledge Xunta de Galicia for the provision of funds 10PXIB103272PR. Collaboration with the University of Oregon was sponsored by the US National Science Foundation, NSF Grant No. CMMI-1069295, and Dr. Mary Toney was the project manager.

REFERENCES

1. Prime, R. B.; Michalski, C.; Neag, C. M. *Thermochim. Acta* **2005**, *429*, 213.
2. Gotor, F. J.; Criado, J. M.; Malek, J.; Koga, N. *J. Phys. Chem. A* **2000**, *104*, 10777.
3. Sańchez-Jiméńez, P. E.; Pérez-Maqueda, L. A.; Perejoń, A.; Criado, J. M. *J. Phys. Chem. A* **2010**, *114*, 7868.
4. Brown, M. E.; Maciejewski, M.; Vyazovkin, S.; Nomen, R.; Sempere, J.; Burnham, A.; Opfermann, J.; Strey, R.; Anderson, H. L.; Kemmler, A.; Keuleers, R.; Janssens, J.; Desseyn, H. O.; Li, C.-R.; Tang, T. B.; Roduit, B.; Malek, J.; Mitsuhashi, T. *Thermochim. Acta* **2000**, *355*, 125.
5. Avrami, M. *J. Chem. Phys.* **1941**, *9*, 177.
6. Avrami, M. *J. Chem. Phys.* **1939**, *7*, 1103.
7. Avrami, M. *J. Chem. Phys.* **1940**, *8*, 212.
8. Farjas, J.; Roura, P. *Acta Mater.* **2006**, *54*, 5573.
9. Johnson, W. A.; Mehl, R. F. *Trans. Am. Inst. Min. Metall. Eng.* **1939**, *135*, 416.
10. Kolmogorov, A. N. "k, Statisticheskoi teori kristallizatsii metallov. *Izv Akad Nayuk CCCR* **1937**, *2*, 355.
11. Vyazovkin, S. In: Handbook of Thermal Analysis and Calorimetry, Elsevier: Amsterdam, 2008; Vol. 5, pp 503–538.
12. Bendall, J. S.; Ilie, A.; Welland, M. E.; Sloan, J.; Green, M. L. H. *J. Phys. Chem. B* **2006**, *110*, 6569.
13. Janković, B.; Adnađević, B.; Jovanović, J. *Thermochim. Acta* **2007**, *452*, 106.
14. Khawam, A.; Flanagan, D. R. *J. Phys. Chem. B* **2006**, *110*, 17315.
15. Milev, A. S.; McCutcheon, A.; Kannangara, G. S. K.; Wilson, M. A.; Bandara, T. Y. *J. Phys. Chem. B* **2005**, *109*, 17304.
16. Premkumar, T.; Govindarajan, S.; Coles, A. E.; Wight, C. A. *J. Phys. Chem. B* **2005**, *109*, 6126.
17. Vyazovkin, S.; Dranca, I. *J. Phys. Chem. B* **2005**, *109*, 18637.
18. Yu, Y.; Wang, M.; Gan, W.; Tao, Q.; Li, S. *J. Phys. Chem. B* **2004**, *108*, 6208.
19. Khawam, A.; Flanagan, D. R. *J. Phys. Chem. B* **2005**, *109*, 10073.
20. Vyazovkin, S. *J. Therm. Anal. Calorim.* **2006**, *83*, 45.
21. Kasap, S. O.; Juhasz, C. *J. Chem. Soc. Faraday Trans. 2* **1985**, *81*, 811.
22. Raju, S.; Mohandas, E. *J. Chem. Sci.* **2010**, *122*, 83.
23. Hemminger, W. F.; Sarge, S. M. *J. Therm. Anal.* **1991**, *37*, 1455.
24. Höhne, G. W. H. *Thermochim. Acta* **1999**, *330*, 93.
25. Perejoń, A.; Sańchez-Jiméńez, P. E.; Criado, J. M.; Pérez-Maqueda, L. A. *J. Phys. Chem. B* **2011**, *115*, 1780.
26. López-Beceiro, J.; Gracia-Fernández, C.; Gómez-Barreiro, S.; Castro-García, S.; Sánchez-Andújar, M.; et al. *J. Phys. Chem. C* **2012**, *116*, 1219.
27. López-Beceiro, J.; Gracia-Fernández, C.; Artiaga, R. *Eur. Polym. J.* **2013**, *49*, 2233.
28. Ferńandez-Francos, X.; Rybak, A.; Sekula, R.; Ramis, X.; Serra, A. *Polym. Int.* **2012**, *61*, 1710.
29. Fernàndez-Francos, X.; Ramis, X.; Serra, A. *J. Polym. Sci. Part A Polym. Chem.* **2014**, *52*, 61.
30. Teil, H.; Page, S. A.; Michaud, V.; Månson, J.-A. E. *J. Appl. Polym. Sci.* **2004**, *93*, 1774.

31. Rocks, J.; Rintoul, L.; Vohwinkel, F.; George, G. *Polymer* **2004**, *45*, 6799.

32. Riccardi, C. C.; Dupuy, J.; Williams, R. J. J. *J. Polym. Sci. Part B Polym. Phys.* **1999**, *37*, 2799.

33. Montserrat, S.; Andreu, G.; Cortés, P.; Calventus, Y.; Colomer, P.; et al. *J. Appl. Polym. Sci.* **1996**, *61*, 1663.

34. Pijpers, T. F. J.; Mathot, V. B. F.; Goderis, B.; Scherrenberg, R. L.; Van der Vegte, E. W. *Macromolecules* **2002**, *35*, 3601.

35. Gracia-Fernández, C.; Tarrío-Saavedra, J.; López-Beceiro, J.; Gómez-Barreiro, S.; Naya, S.; et al. *J. Therm. Anal. Calorim.* **2011**, *106*, 101.

36. Artiaga, R.; López-Beceiro, J.; Tarrío-Saavedra, J.; Gracia-Fernández, C.; Naya, S.; et al. *J. Chemom.* **2011**, *25*, 287.

37. Artiaga, R.; Naya, S.; Cao, R.; Barbadillo, F.; Fuentes, A. Polymer Degradation and Stability Research Developments, Nova Science Publishers: New York, **2007**.

38. Cao, R.; Naya, S.; Artiaga, R.; García, A.; Varela, A. *Polym. Degrad. Stab.* **2004**, *85*, 667.

39. Naya, S.; Cao, R.; de Ullibarri, I. L.; Artiaga, R.; Barbadillo, F.; et al. *J. Chemom.* **2006**, *20*, 158.

40. Wojdyr, M. *J. Appl. Crystallogr.* **2010**, *43*, 1126.